


Unified scale laws for transient convective boundary layers: From flat to curved boundary layers

Yang Liu* and Changhui Liu *School of Ocean Science and Technology, Dalian University of Technology, Dalian, 116024, China*

(Received 28 October 2021; accepted 18 April 2022; published 2 May 2022)

Temporally evolving convective boundary layers that develop on the external surface of an isothermally heated vertical circular cylinder are investigated with scale analysis in this study. Large variation of cylinder aspect ratio, $1 \leq A \leq 100$, is considered. The Rayleigh number ranges from 1×10^6 to 5×10^8 , and the Prandtl number varies from 10 to 100. The present numerical simulations suggest that the curved boundary layer experiences a transient and a steady state. Our study demonstrates that the key to correctly scaling the curvature effect is the determination of an appropriate estimation of the diffusion term. One set of scale laws quantifying the flow is obtained by assuming $(1/r)(\partial/\partial r) \sim 1/[(R + \delta/2)\delta]$, where r is the radial coordinate, and R and δ denote cylinder radius and boundary layer thickness, respectively. It is demonstrated that if the boundary layer is much thinner than the cylinder radius, the proposed scale laws are reduced to the well-known flat boundary layer ones. However, with reducing the cylinder radius or the governing Rayleigh number, the curvature effect gradually differentiates the present boundary layer flow from the flat ones. The corresponding flow behaviors are reasonably described by the various $(R + N\delta)^m$ terms of the present scale laws, where N and m are the corresponding scale-law constants. Numerical validations indicate that the proposed scale laws are capable of precisely describing from flat boundary layers at $\xi = 0$ to remarkably curved ones at $\xi = 26$ (almost a line heat source), where ξ is the ratio of boundary layer thickness to cylinder radius. Therefore, the proposed scale relations are considered as unified laws.

DOI: [10.1103/PhysRevFluids.7.054101](https://doi.org/10.1103/PhysRevFluids.7.054101)

I. INTRODUCTION

Natural convection boundary layer flow is a ubiquitous problem of great interest to fluid mechanics [1], with many industrial, atmospheric, and geophysical applications. Existence and structure of boundary layers were first identified and reported by Prandtl [2]. Soon after that, a two-dimensional boundary layer flow developing on a semi-infinite plate was studied by Blasius [3]. Batchelor pioneered cavity studies by investigating a buoyancy-driven flow across a closed rectangle enclosure between two vertical boundaries at different temperatures [4]. Subsequently, many aspects of the natural convection boundary layer flow have been extensively investigated and documented in the literature; see, e.g., [5–7]. In the last several decades, the unprecedented development in semiconductor equipment, hot filaments, and heat loss of various tanks in the crude and ocean thermal energy conversion (OTEC) industries urgently demanded better understanding of curved boundary layer flows; see, e.g., [8–10]. The present study is in fact illuminated by the request to maintain the temperature of an icebreaker ship using vertically arranged cylindrical heat radiators. The prototype of the industrial radiator adopts the general form of domestic ones, where

*yang.liu1@qq.com; yangliu1@dlut.edu.cn

the corresponding Ra is approximately 2×10^8 , the typical aspect ratio of the heated cylinder is around 20, and the Prandtl number of the fluid is around 10.

Over the years, the curved boundary layer flows have indeed attracted some attention. However, most of the documented works in the literature focused on the associated heat transfer properties. That was to determine how the Nusselt number is correlated with the characterizing Rayleigh number and geometrical dimensions of the vertical cylinder. Langmuir [11] carried out the first experiment and confirmed the effect of curvature. Elenbaas [12] employed Langmuir's stagnant film model and predicted the heat transfer coefficient for vertical cylinders by replacing the natural convection problem with a heat conduction problem. The transient and steady-state temperatures of thin vertical cylinders suspended in various fluids were measured by Dring and Gebhart [13]. The experimental data confirmed that the conduction theory could properly address the transient temperature response of the cylindrical wires. Minkowycz and Sparrow [14] successfully applied the local nonsimilarity solution method to account for the natural convection flow on a vertical cylinder for fluids with $Pr = 0.733$. Khouaja *et al.* [15] further studied the mixed convection flow along slender vertical cylinders that are subjected to heat flux conditions. The authors demonstrated that the Nusselt number results could be calculated by the summation of the local Nusselt number for pure natural convection and that for pure forced convection. In comparison to the various attempts of determining the scale of the Nusselt number, flow characteristics of the curved boundary layer were relatively less discussed. Recently, Zhao *et al.* [16] investigated the steady-state curved boundary layer on a vertical cylinder, and the authors indicated that thickness and Nusselt number of the curved boundary layer vary according to $Ra^{-1/5}$ and $Ra^{1/5}$, respectively. However, several previous works argued that an exponent $1/4$ is more appropriate; see, e.g., [12, 17]. This discrepancy suggests that flow behaviors of the curved boundary layer on a circular cylinder have not yet been thoroughly understood by the convection community, which is mainly attributed to the fact that the flow behavior greatly depends on the curvature of the heated surface.

The so-called flow scale analysis, among many others, is considered a highly inspiring, useful, and powerful technique to understand the corresponding flow behaviors, and there are mainly two popular types of scale analysis in the literature.

The first type is a derivation-based approach where scales describing the natural convection flow are determined by analyzing the governing equations of the flow. This type of scaling analysis is most frequently utilized to study the flow with a distinct boundary layer. As is widely known, the general form of governing equations for any flow variable ϕ could be written as $\partial\phi/\partial t + \vec{V} \cdot \vec{\nabla}\phi = \Gamma\nabla^2\phi + s$. By analyzing the various terms and choosing dominant ones at different flow states, the corresponding flow scales could be subsequently obtained. This simple scaling methodology was pioneered by Patterson and Imberger [1], Bejan [18], and others. Patterson and Imberger [1] studied the natural convection flow in a differentially heated cavity for fluids at $Pr > 1$, where important scales were obtained. Bejan [18] suggested that the Boussinesq number Bo , rather than the Rayleigh number, is the more appropriate governing parameter for $Pr < 1$ fluids. Lin *et al.* [19] revisited and analyzed the $Pr > 1$ fluids, and the Prandtl number dependency was successfully obtained. Recently the convective boundary layer flows induced by a linear thermal forcing at the heated surface were intensively studied in [20–22]. The authors demonstrated that unlike the homogeneously heated problems, the initial growth of the thermal boundary layer becomes two-dimensional. Apart from the above isothermally heated problems, evenly heated flat boundary layers have also been extensively studied over the years; see, e.g., [23–27].

The second type of scale analysis is generally based on data processing, where scales quantifying the convective flow are obtained either by regressing simulation data or by fitting experimental data. This branch of scaling analysis is usually employed to study relatively complex convection flows that have no distinct boundary layer or a discernible interface, for instance, the Rayleigh-Taylor instability and Rayleigh-Bénard convection. The $Nu \sim Ra$ dependency was obtained at the interface of two fluids with different densities in [28]. Celani *et al.* [29] demonstrated that the transient Nusselt and Reynolds numbers scale with the square root of the Rayleigh number.

Boffetta *et al.* [30] showed that the Reynolds and Nusselt numbers change with the Rayleigh number according to $Nu \sim Pr^{1/2}Ra^{1/2}$ and $Re \sim Pr^{-1/2}Ra^{1/2}$, respectively, which agree well with [29] and [31]. Dependency of the Nusselt number on the Rayleigh number has been an everlasting topic of the Rayleigh-Bénard convection problem. Among many others, [32] proposed the scale laws $Nu \sim Pr^0Ra^{1/3}$ and $Re \sim Pr^{-1}Ra^{2/3}$ for the thermal convection flow, which were later confirmed in [33]. Later, Miquel *et al.* [34] suggested that the scaling regime $Nu \sim Ra$ of the asymptotic solution corresponds to a maximization of the heat flux for thermal convection driven by internal sources. Recently, wall-bounded turbulent flows were studied by the scaling analysis in [35,36] where Reynolds stresses and kinetic energy were appropriately described by the proposed scale laws.

The above literature review suggests that scale laws of cylindrical boundary layers have not been obtained previously. Intuitively, natural convection boundary layers at an adequately high Rayleigh number or on a cylindrical surface of a sufficiently large radius should behave similarly to those develop on a flat plate. However, the curvature effect becomes increasingly crucial as the radius of the heated cylinder decreases. The present scale-law investigation essentially inherits the scaling of flat boundary layer studies but is dedicated to resolving the curvature effect of a heated cylindrical surface. The traditional flat boundary layer scalings will be reduced to one limiting scenario of the present scale laws. To the authors' best knowledge, this is the first time that these results are reported in the literature. It is also worth clarifying that in comparison to the work in Zhao *et al.* [16], we aim to further analyze the transient state, elucidate the corresponding scale laws, especially the exponents at both transient and steady states, and propose a set of unified scale laws as our ultimate goal.

The present study investigates the temporally evolving curved boundary layer around the external surface of an isothermally heated vertical circular cylinder and obtains a set of unified scale laws to account for the curvature and Rayleigh and Prandtl number dependencies. In the present study, both the transient and steady states are studied to reveal the corresponding fundamental fluid mechanics. It is worth noting that the present scale-law study aims to obtain a set of scale laws that could describe flow behaviors in different flow scenarios rather than investigating the flow characteristics at a specific flow condition as is usually seen in simulation-based works.

In the remainder of this paper, Sec. II describes the flow and governing equations followed by scale-law analysis in Sec. III. Validations of the proposed scale laws are given in Sec. IV. The main conclusions of this work are summarized in Sec. V.

II. PHYSICAL PROBLEM AND NUMERICAL METHODS

Under consideration is a laminar convective boundary layer flow developing on a heated vertical cylinder. Height and radius of the vertical cylinder are L and R , respectively. It is noted that in the present study, L is fixed at 1 m. Therefore, by adopting the different aspect ratio A , the radius of the cylinder is changed accordingly, which will subsequently alter the curvature of the heated surface. It is worth noting that the following scale-law study is carried out in a dimensional scheme, and this is consistent with [1,37].

At a time instance $t < 0$ s, the fluid is quiescent and the temperature is kept at T_0 , whereas the circular cylinder is also isothermal at T_0 . At $t = 0$ s, temperature of the cylinder surface is suddenly raised to T_w ($T_w > T_0$), and it is maintained thereafter. The increase in temperature initiates and sustains the boundary layer flow on the external surface of the cylinder.

The convective flow around the external surface of the circular cylinder could be described by the following governing equations for boundary layer with the Boussinesq approximation for the buoyancy term:

$$\frac{1}{r} \frac{\partial r u_r}{\partial r} + \frac{\partial u_z}{\partial z} = 0, \quad (1)$$

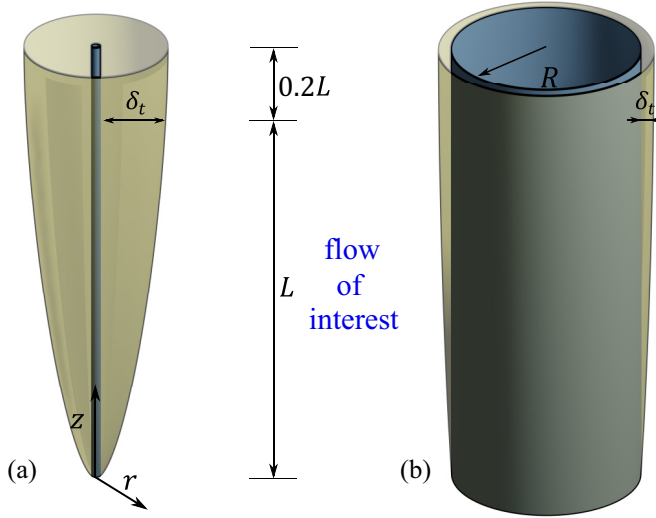


FIG. 1. Two typical flow scenarios depicting the effect of curvature on the convective boundary layer at $Pr = 10$: (a) a strongly curved boundary layer where δ_t equals approximately $14R$ at $z = L$ ($Ra = 10^6$ and $A = 100$); (b) an almost flat boundary layer where δ_t equals approximately $0.12R$ at $z = L$ ($Ra = 5 \times 10^8$ and $A = 5$).

$$\frac{\partial u_z}{\partial t} + u_r \frac{\partial u_z}{\partial r} + u_z \frac{\partial u_z}{\partial z} = \nu \frac{1}{r} \frac{\partial}{\partial r} \left(r \frac{\partial u_z}{\partial r} \right) + g\beta(T - T_0), \quad (2)$$

$$\frac{\partial T}{\partial t} + u_r \frac{\partial T}{\partial r} + u_z \frac{\partial T}{\partial z} = \kappa \frac{1}{r} \frac{\partial}{\partial r} \left(r \frac{\partial T}{\partial r} \right), \quad (3)$$

where u_r and u_z denote the velocity components in the radial and axial directions, respectively. In the present study, the convective boundary layer flow is governed by three parameters: the Rayleigh number Ra , Prandtl number Pr , and aspect ratio A of the cylinder (or cylinder radius R). They are defined as

$$Ra = \frac{g\beta\Delta TL^3}{\nu\kappa}, \quad Pr = \frac{\nu}{\kappa}, \quad A = \frac{L}{R}, \quad (4)$$

where g , β , ν , and κ are the gravitational acceleration, thermal expansion coefficient, kinematic viscosity, and thermal diffusivity of the working fluid, respectively. ΔT is the temperature difference characterizing the convective flow, which is defined by $\Delta T = (T_w - T_0)$.

Figure 1 schematically shows the thermal boundary layers at two typical flow conditions. It is seen that the leading edge of the boundary layer is at $z = 0$ and the boundary layer thickens with the streamwise coordinate z . It is also seen in Fig. 1 that the present boundary layer could be much thicker or much thinner than the radius of the cylinder. Note that Fig. 1(a) corresponds to the most curved boundary layer under investigation, and Fig. 1(b) stands for the second least curved boundary layer.

The present study utilizes the so-called scale-law analysis to investigate the boundary layer flow, which is mainly by analyzing the various force and momentum terms of the governing Eqs. (1)–(3). Nonetheless, to validate the obtained scale laws, a numerical approach needs to be employed, where the governing equations are accounted for by the finite volume method (FVM). All the first linear and second derivative terms of the governing equations are spatially discretized by a

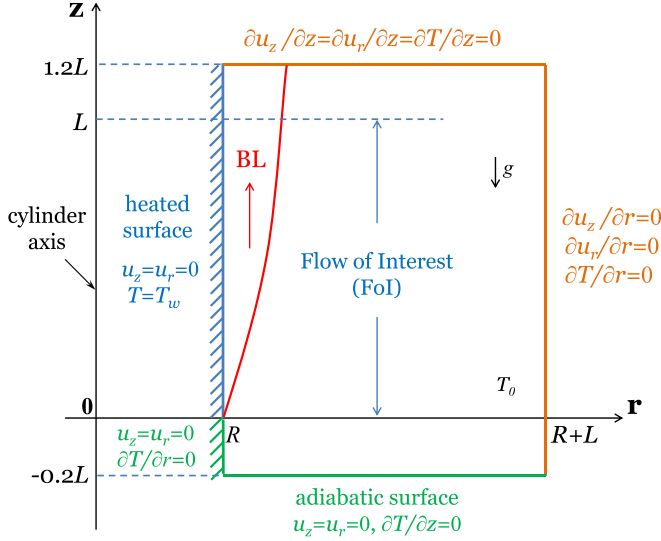


FIG. 2. Schematic of the computational domain.

second-order central differencing scheme. The first-order implicit method is employed to approximate the transient terms. The pressure and velocity correlation utilizes the SIMPLE scheme. The governing equations are then solved iteratively by incorporating a third-order Runge-Kutta scheme. The solution is regarded converged when the scaled residual falls below 10^{-3} for the continuity and momentum equations and 10^{-6} for the temperature equation. These numerical procedures are essentially similar to those adopted in [20,21]. It is worth noting that the present code has been intensively utilized in the past decade for various buoyancy-driven convective flows, and it has been proven accurate and robust; see, e.g., [20,37,38]. It is hence used in this study.

In this study, a two-dimensional model is employed for the numerical simulations. Figure 2 schematically shows the adopted computational domain. It is seen that z and r represent stream-wise/axial and radial directions, respectively. The height of the entire computational domain is $1.4L$. The boundary layer evolves from $z = 0$, which corresponds to its leading edge location. An adiabatic extension and another heated extension of length $0.2H$ is considered at the upstream and downstream of the boundary layer flow respectively to avoid any potential effects that might be caused by the boundaries. Therefore, the length of flow of interest to the present study is L , $0 < z < L$. In the radial direction, $r = 0$ corresponds to the axis of the heated cylinder and the width of the computational domain is also L . At the top and right boundaries, a nonreflective boundary condition is employed. The present computational domain and the adopted boundary conditions are essentially the same as those adopted in [7,21,23,24], and these works suggested that the combination of two Neumann boundaries and the employed computational domain could be properly utilized for the boundary layer flow under investigation.

It is worth mentioning that the Cartesian coordinate is extensively utilized for flat boundary layer problems and hereby not employed for the present study. Alternatively, the cylindrical coordinates which could better facilitate descriptions of cylindrical boundary layer variables and the subsequent derivations of the corresponding scaling laws are used. It is also worth clarifying in Fig. 2 that when the cylinder radius R changes, it affects several advection and diffusion terms in the corresponding governing equations, and subsequently, the curvature effect is taken into account. This numerical approach is in fact consistent with [9,16].

A total of 84 numerical simulations have been carried out to validate the above derived scale laws. The Rayleigh number varies from 1×10^6 to 5×10^8 . At each Rayleigh number, three Prandtl numbers and seven aspect ratios, A , are calculated. Table I details the utilized parameters. It is

TABLE I. Flow parameters of the simulated case runs.

Case runs	Ra	$A = L/R$	Pr
1–21	10^6	100, 50, 20, 10, 5, 2, 1	10, 40, 100
22–42	10^7	100, 50, 20, 10, 5, 2, 1	10, 40, 100
43–63	10^8	100, 50, 20, 10, 5, 2, 1	10, 40, 100
64–84	5×10^8	100, 50, 20, 10, 5, 2, 1	10, 40, 100

worth repeating that L does not vary in this study, and by adopting different cylinder aspect ratios, the radius of the cylinder is subsequently changed. Herein, the aspect ratio A varies from 100 to 1, and this corresponds to a minimum radius $R = 0.01L$ and a maximum radius $R = L$. That is, the radius of the heated cylinder is very small at $A = 100$, and this is associated with the most significantly curved boundary layer (the following numerical data suggest that $\delta_t|_{\text{maximum}} \sim 14R$ in this scenario). $A = 1$ corresponds to a very large radius, and this value results in a much less curved boundary layer that is almost equivalent to the flat-plate problem (the following numerical data suggest that $\delta_t|_{\text{minimum}} \sim 0.02R$ in this scenario).

To ensure the adopted numerical settings do not affect the accuracy of simulations, grid and time step dependency tests are carried out. In this study, three meshes and three time steps are employed for this purpose. The three sets of computational mesh consist of 300×600 , 200×426 , and 100×213 quadrilateral cells ($r \times z$), respectively. The size of the grid immediately adjacent to the heated cylinder surface is 0.1 mm, 0.17 mm, and 0.21 mm, and the computational cell stretches linearly towards the ambient at an inflation rate of 1.09, 1.1, and 1.3, respectively, for the three meshes. This corresponds to no fewer than 34, 29, and 27 grids within the convective thermal boundary layer, which, according to previous similar studies, are sufficient to resolve the present boundary layer flow; see, e.g., [20,23,37]. It is also worth pointing out that the grid is evenly spaced in the streamwise direction, i.e., in the z direction. Three time steps, $\Delta t = 0.0025$ s, 0.005 s, and 0.01 s, are further examined to guarantee the present numerical results are time step independent. During transient calculations of the governing Eqs. (1)–(3), the characteristic velocity and thickness of the convective boundary layer are monitored and recorded at $z = L$ for the case with $\text{Ra} = 5 \times 10^8$, $\text{Pr} = 100$, and $A = 100$. Figure 3(a) presents the corresponding results. Note that δ_i is identified at $(T_w - \Delta T \times 0.99)$, and the maximum streamwise velocity within the thermal boundary layer is recognized as u_z . It is seen that the variations are quite minor. The maximum relative error is approximately 0.075% and 0.15% for the characteristic velocity and thickness of the steady-state convective boundary layer, respectively. This suggests that any of the utilized grids and time steps could be employed. Hence, the mesh with 200×426 computational cells together with the time step 0.005 s is adopted for the following numerical simulations.

Temporal evolution of isotherms adjacent to the heated surface is depicted in Fig. 3(b). It is seen that the boundary layer development is one-dimensional in the first place, which is evidenced by the fact that its thickness is streamwise independent at $t = 0.5$ s, 1 s, and 1.5 s. It also demonstrates that two-dimensional growth sets in when t exceeds 2.5 s, and thereafter the boundary layer thickness depends on the streamwise location. It is noted that the r coordinate in this figure is rescaled with a factor of 4 to produce a better view of the extremely thin boundary layer. The corresponding temporal and spatial development of velocity vectors are shown in Fig. 3(c). It is seen that the local velocity u_z first increases in the r direction due to the buoyancy effect, and it then reduces towards the ambient. At each streamwise location, e.g., $y = 1$, the velocity increases temporally until it reaches a threshold time instance, after which it does not vary with time any longer. This flow structure is essentially the same as the extensively investigated flat boundary layer; see, e.g., [1,18,19].

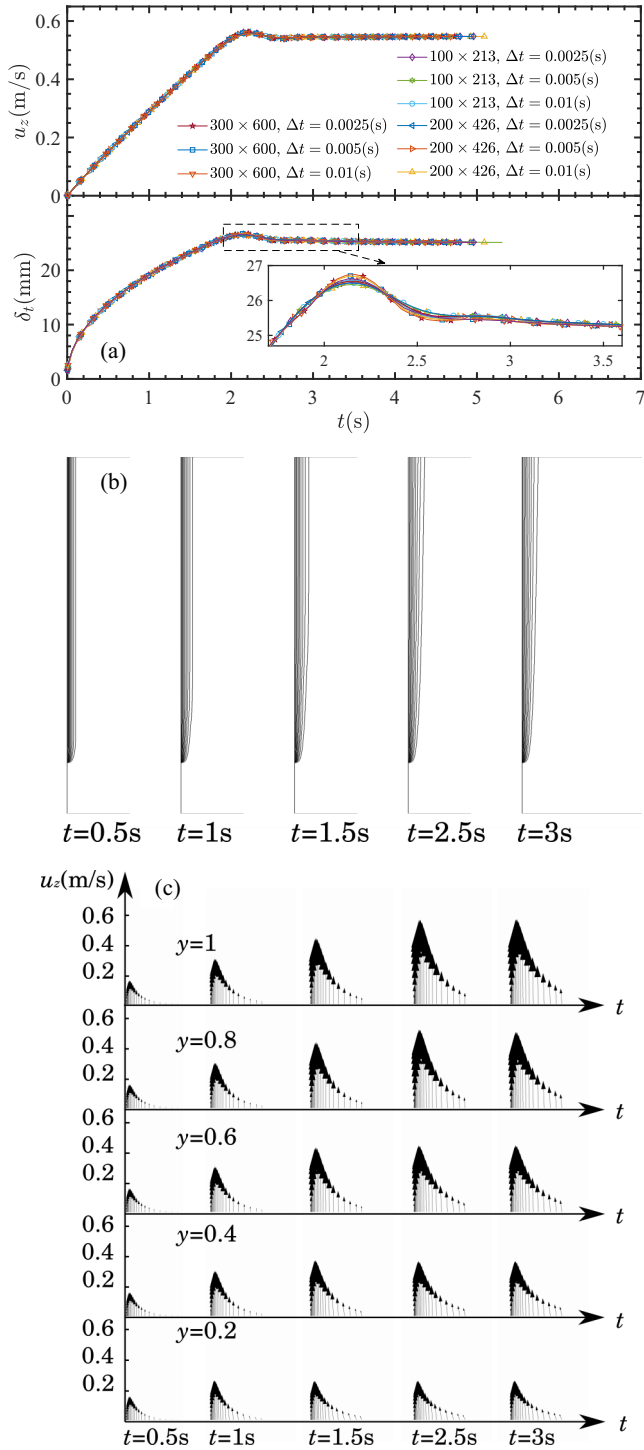


FIG. 3. Grid and time step dependency tests: temporal development of u_z and δ_t of the thermal boundary layer at $Ra = 5 \times 10^8$, $Pr = 100$, and $A = 100$. (a) Comparison between different meshes and time steps, (b) isotherms obtained with 200×426 and $\Delta t = 0.005$ s, (c) velocity vector obtained with 200×426 and $\Delta t = 0.005$ s.

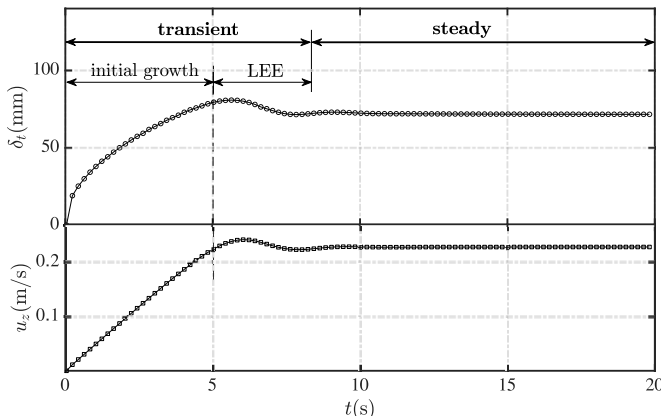


FIG. 4. Temporal development of the thickness and characteristic velocity of the curved boundary layer with $Ra = 1 \times 10^7$, $Pr = 10$, and $A = 100$, monitored and recorded at a streamwise location $z = L$.

III. SCALE-LAW ANALYSIS

For the extensively studied boundary layer flow along a heated vertical flat plate (flat-plate problems), we could easily reach $u_z \delta_t \sim u_r L$ from the continuity equation, where u_z and u_r denote the characteristic velocity of the vertical thermal boundary layer flow and the weak horizontal entraining flow from the ambient. This reveals the flow rate of the boundary layer equals the entraining flow flux. Moving on from this, we could write $2\pi(R + \delta_t)Lu_r \sim 2\pi(R + \delta_t/2)\delta_t u_z$ for the present study, where $2\pi(R + \delta_t)L$ is the surface area of the characteristic cylindrical boundary layer and $2\pi(R + \delta_t/2)\delta_t$ denotes the cross-sectional area of the boundary layer annulus. Therefore, we could arrive at

$$u_r \sim u_z \frac{\delta_t R + \delta_t/2}{L R + \delta_t}. \quad (5)$$

Equation (5) could also be rearranged in the form of Eq. (1) as

$$\frac{1}{R + \delta_t/2} \frac{1}{\delta_t} (R + \delta_t) u_r + \frac{u_z}{L} \sim 0. \quad (6)$$

A comparison of Eq. (1) against Eq. (6) suggests that the proper estimation of the differential operator $(1/r)(\partial/\partial r)$ in the cylindrical coordinate system may adopt the form $1/[(R + \delta_t/2)\delta_t]$. This will be utilized in the following analysis. It is noted that the scaling methodology does not account for the sign of the various terms, and it focuses only on order of magnitude of the terms [1].

Figure 4 shows the numerically determined thickness δ_t and characteristic velocity u_z of the curved boundary layer at a typical flow condition with $Ra = 1 \times 10^7$, $Pr = 10$, and $A = 100$. Three distinct development states are clearly demonstrated in this figure, which consists of an initial unsteady growth, a leading-edge-effect (LEE) dominated oscillatory state, and a steady state. The first two states could be grouped and treated as a transient state. This flow evolution is essentially the same as the extensively investigated flat-plate boundary layers. In what follows, the scale analysis will be separately carried out for the transient state and the fully developed state.

A. Initial growth

Immediately after the circular cylinder is heated, the boundary layer flow is initiated, and it is dominated by heat conduction in the first place. In the energy Eq. (3), the transient time $\partial T/\partial t$ is larger than the advection term before the boundary layer reaches its steady state. Therefore, we

could write the following balance:

$$\frac{\partial T}{\partial t} \sim \kappa \frac{1}{r} \frac{\partial}{\partial r} \left(r \frac{\partial T}{\partial r} \right). \quad (7)$$

Similar to the thermal boundary layer at vertical flat plates, the first derivative $\partial T/\partial t$ is estimated by $\Delta T/t$. Note that in the present study, curvature of the cylinder could significantly “bend” the boundary layer towards the cylinder surface, and it hereby spatially alters the profile of temperature and velocity within the boundary layer. Consequently, the derivative term $(r\partial T/\partial r)$ cannot be simply quantified by $R\Delta T/\delta_t$. However, it is worth noting that estimating $(r\partial T/\partial r)$ by $R\Delta T/\delta_t$ is a routine for boundary layer flows developing at vertical flat plates. In this study, to account for the curvature effect in the circumferential direction, the numerator r in $(r\partial T/\partial r)$ is alternatively estimated by R_1 , and it is to be determined by the radius R and δ_t . Therefore, by considering and incorporating the estimation of $r\partial T/\partial r$, Eq. (7) could be recast as

$$\frac{\Delta T}{t} \sim \kappa \frac{1}{(R + \delta_t/2)} \frac{1}{\delta_t} \frac{R_1 \Delta T}{\delta_t}, \quad (8)$$

which gives

$$\delta_t^2 \sim \kappa t \frac{R_1}{R + \delta_t/2}. \quad (9)$$

We assume the coefficient R_1 in Eq. (9) is in the form $R + C_1\delta_t$. Owing to the curving nature of the boundary layer, the constant C_1 has to be determined from the present numerical simulations, more specifically, from seven cases with a Rayleigh number 10^8 , Prandtl number 10, and L/R ranging from 100 to 1. To achieve this, the following function Ψ_1 is defined:

$$\Psi_1(C_1) = \frac{\delta_t \left(\frac{R + 0.5\delta_t}{R + C_1\delta_t} \right)^{1/2}}{\kappa^{1/2} t^{1/2}}. \quad (10)$$

In Eq. (10), $\kappa^{1/2} t^{1/2}$ is a known and definitive value at any evolutionary time instant t . The value of the term $\delta_t(R + 0.5\delta_t)^{1/2}/(R + C_1\delta_t)^{1/2}$ depends on C_1 . Different C_1 values will lead to different Ψ_1 , and the primary task here is to find an appropriate C_1 value that could best describe the present boundary layer thickness at different flow conditions. Note that at any specific C_1 , the value of Ψ_1 is calculated at 70 data points during the transient calculations, which comprise ten evolutionary times t and seven aspect ratios L/R . Subsequently, the standard deviation of $\Psi_1|_{C_1}$ could be determined from the 70 data clusters. Figure 5 summarizes and compares $\sigma(\Psi_1)$, the standard deviation of Ψ_1 , obtained at 100 C_1 values ranging from 0 to 2 with a uniform step of 0.02. It is clear in this figure that $\sigma(\Psi_1)$ hits its minimum at approximately $C_1 = 0.3$. This suggests that this particular C_1 is the most appropriate value, and C_1 is hence determined to be 0.3. It is worth noting at this point that to be more rigorous, we compare the $\sigma(\Psi_1)$ curve determined at $Ra = 10^8$ and $Pr = 10$ against that obtained for all 84 cases considered in this study. It is obviously demonstrated in Fig. 5 that both data suggest $C_1 = 0.3$ corresponds to the minimum deviation and hence it is the most appropriate value. In other words, the determined coefficient is Ra and Pr independent. Our following results in the validation section also demonstrate that an identical C_n exists for different Ra and Pr ; therefore, we utilize only the data at $Ra = 10^8$ and $Pr = 10$ in this section, in Figs. 5–9. Therefore, δ_t could be quantified by the following:

$$\delta_t \left(\frac{R + 0.5\delta_t}{R + 0.3\delta_t} \right)^{1/2} \sim \kappa^{1/2} t^{1/2}. \quad (11)$$

It is clear that the above scale relation is not in the directly explicit form that is commonly seen for thermal boundary layers at vertical flat plates, and the complexity of Eq. (11) demonstrates the effect of curvature and its difference from vertical flat ones. This equation strongly implies three

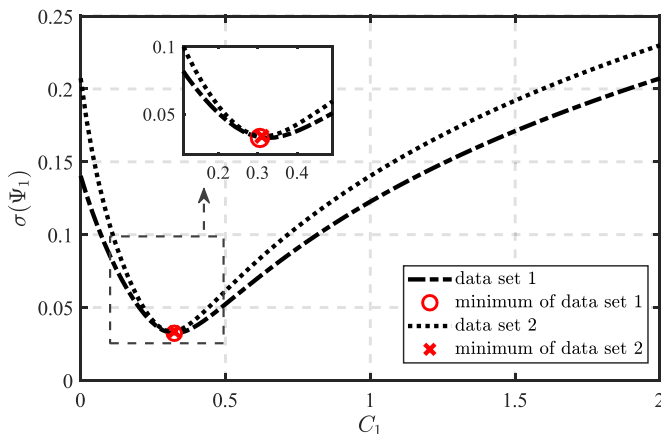


FIG. 5. $\sigma(\Psi_1)$ plotted vs C_1 for the cases with data set 1 ($Ra = 1 \times 10^8$, $Pr = 10$, and $1 \leq A \leq 100$) and data set 2 (at 4 Ra , 3 Pr , and 7 A).

scenarios for the curved thermal boundary layer. First, if the radius of the circular cylinder is much larger than the thickness of the boundary layer, the problem is subsequently reduced to the flat plate problems, and Eq. (11) will become the well-known $\delta_t \sim \kappa^{1/2} t^{1/2}$ relation. Second, in the case of a very small radius, δ_t will be much larger than R , and the scale relation will also tend to approach $\delta_t \sim \kappa^{1/2} t^{1/2}$. Third, if δ_t and R are comparable, the term $(R + 0.5\delta_t)/(R + 0.3\delta_t)$ does not converge to any specific value. Alternatively, it indicates the underlying interplay between the two parameters and hereby reflects the effect of the curvature of the circular cylinder in this competing scenario. Nevertheless, the most important thing here is that the proposed Eq. (11) gives unified predictions of the initial growth of the boundary layer thickness covering a large range of δ_t/R .

For the thermal boundary layer flow at vertical flat plates, the scale $\delta_t \sim \kappa^{1/2} t^{1/2}$ is used to quantify the temporal development of its thickness. Hence, we could estimate the thickness of the boundary layer flow at any evolutionary time t with this scaling law in a straightforward way. That is, for example, at a given time instance t , one could easily obtain the value of $\kappa^{1/2} t^{1/2}$. Nevertheless, Eq. (11) demonstrates that to precisely include the present curvature effect, an additional term needs to be considered, and the term $\delta_t(R + 0.5\delta_t)^{1/2}/(R + 0.3\delta_t)^{1/2}$, rather than δ_t , correlates with $\kappa^{1/2} t^{1/2}$. Mathematically, the scale relation in Eq. (11) will reduce to $0.5\delta_t^3 + R\delta_t^2 - 0.3\kappa t\delta_t - \kappa tR \sim 0$.

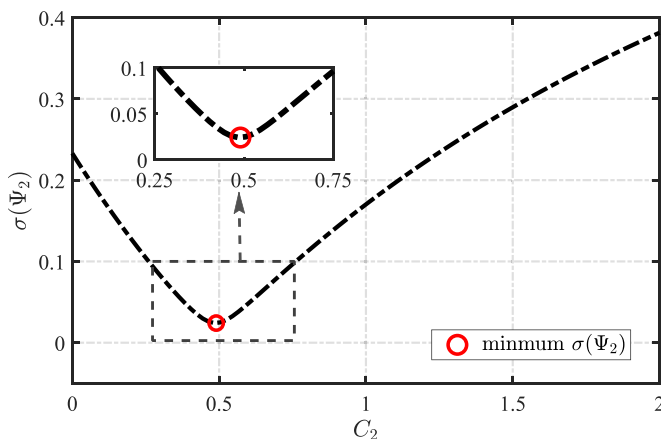


FIG. 6. $\sigma(\Psi_2)$ plotted vs C_2 for the cases with $Ra = 1 \times 10^8$, $Pr = 10$, and $1 \leq A \leq 100$.

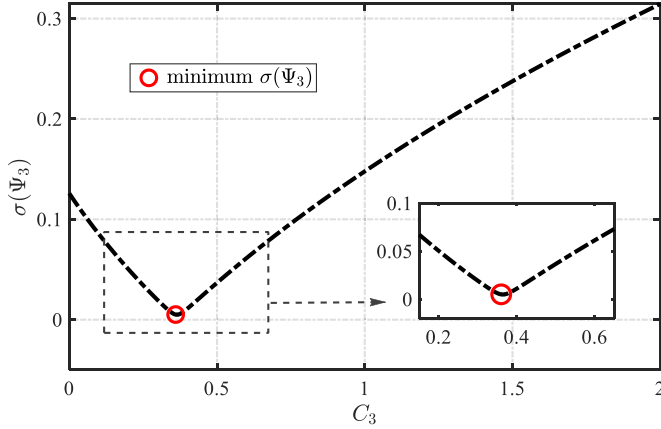


FIG. 7. $\sigma(\Psi_3)$ plotted vs C_3 for the cases with $Ra = 1 \times 10^8$, $Pr = 10$, and $1 \leq A \leq 100$.

However, it could not lead to a unique δ_t value as the intercept is not fixed. Also, several subsequent scale laws are not possible without determination of an exact solution of δ_t . This implicit style of δ_t suggests that to obtain an estimation of δ_t at a specific time t in the initial growth state, which is usually desired by the convection community, Eq. (11) needs to be accounted for iteratively. In this respect, the order of magnitude sign in Eq. (11) must be replaced by an equal sign. The exact form of Eq. (11) is determined from our numerical simulations of the seven cases at a Rayleigh number 10^8 , Prandtl number 10, and L/R ranging from 100 to 1. Regression analysis is carried out for the simulation data, and it is found that a coefficient 3.7 is appropriate and the associated R^2 is 0.997. Then, we could come to the following Eq. (12):

$$\delta_t \left(\frac{R + 0.5\delta_t}{R + 0.3\delta_t} \right)^{1/2} = 3.7\kappa^{1/2}t^{1/2}. \quad (12)$$

Buoyancy drives the curved convective boundary layer flow. Therefore, $g\beta\Delta T$ must present and dominate the momentum of the flow in Eq. (2). As suggested by Patterson and Imberger [1], the viscous force is more significant than the inertial effect for the present fluids at $Pr \gg 1$. Therefore,

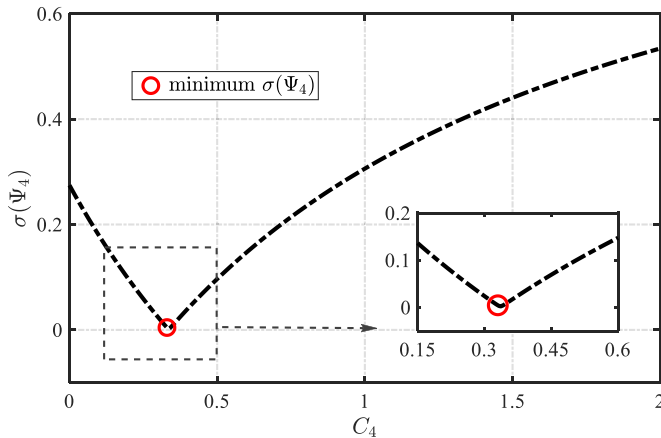


FIG. 8. $\sigma(\Psi_4)$ plotted vs C_4 for the cases with $Ra = 1 \times 10^8$, $Pr = 10$, and $1 \leq A \leq 100$.

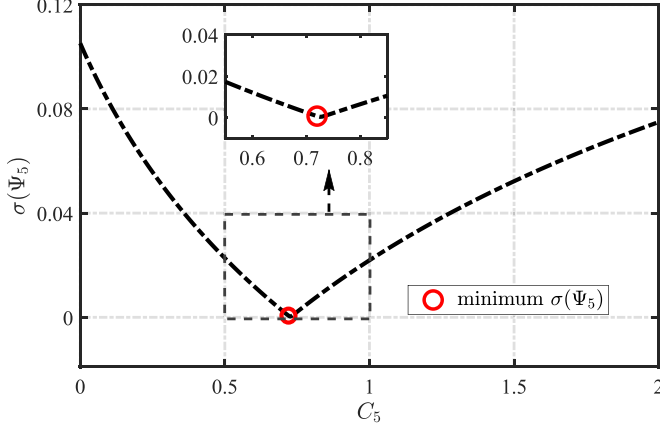


FIG. 9. $\sigma(\Psi_5)$ plotted vs C_5 for the cases with $Ra = 1 \times 10^8$, $Pr = 10$, and $1 \leq A \leq 100$.

we could write

$$g\beta\Delta T \sim v \frac{1}{r} \frac{\partial}{\partial r} \left(r \frac{\partial u_z}{\partial r} \right). \quad (13)$$

By adopting an analogy to the above employed techniques for deriving δ_t , Eq. (13) could be rewritten as

$$g\beta\Delta T \sim v \frac{1}{(R + 0.5\delta_{vi})} \frac{1}{\delta_{vi}} \frac{R_2 u_z}{\delta_{vi}}, \quad (14)$$

where R_2 denotes the circumferential effect caused by the curved surface, and it assumes the form $R_2 = R + C_2\delta_{vi}$. Due to the viscous effect, the local velocity adjacent to the heated surface maximizes at $R + \delta_{vi}$, where δ_{vi} is the thickness of the inner viscous layer. It is crucial to mention here that, in addition to utilizing the operator $(1/r)(\partial/\partial r) \sim 1/[(R + \delta_{vi}/2)\delta_{vi}]$, we use δ_{vi} as the length scale for the momentum equation, while many previous scaling investigations employed δ_t for both the momentum and energy equations. Our study suggests that the correct velocity scale and Prandtl number effect will not be obtained by utilizing δ_t , and employing δ_{vi} for the momentum equation is in fact consistent with the work in [19]. The authors also suggested that δ_{vi} could be described by $\delta_{vi} \sim \delta_t/(1 + Pr^{-1/2})$ for the present $Pr \gg 1$ fluids [19]. Similar to the above technique of deciding C_1 for the boundary layer thickness, Fig. 6 compares the standard deviation of the function Ψ_2 expressed in Eq. (15):

$$\Psi_2(C_2) = \frac{\frac{g\beta\Delta T t}{(1+Pr^{1/2})^2} \left(\frac{R+0.5\delta_{vi}}{R+C_2\delta_{vi}} \right) \left(\frac{R+0.3\delta_t}{R+0.5\delta_t} \right)}{u_z}. \quad (15)$$

Note that C_2 is also determined from the numerical simulations with the seven case runs at a Rayleigh number 10^8 , Prandtl number 10, and L/R from 100 to 1. Figure 6 demonstrates that C_2 is determined to be 0.5. Hence, Eq. (14) becomes

$$u_z \sim \frac{g\beta\Delta T t}{(1 + Pr^{1/2})^2} \left(\frac{R + 0.3\delta_t}{R + 0.5\delta_t} \right). \quad (16)$$

Equation (16) demonstrates that the characteristic velocity in the thermal boundary layer is not an explicit relation as well. To obtain the scale-law-predicted u_z , the thickness of the thermal boundary layer has to be determined prior. Likewise, the term $(R + 0.3\delta_t)/(R + 0.5\delta_t)$ in Eq. (16) suggests the curvature effect of the heated surface. That is, for cylinders with a sufficiently large or a sufficiently small radius, u_z could be simply described by a recast version of the scale relation (16),

$(Ra\kappa^2 t)/[L^3(1 + Pr^{-1/2})^2]$, which is the widely utilized velocity scale for flat-plate boundary layers proposed in [19]. In comparison, the term $(R + 0.3\delta_t)/(R + 0.5\delta_t)$ acts to calibrate a flat plate scale law towards a curved one.

With the passage of time, convection gradually improves, and the boundary layer flow reaches a steady state at t_s , from which time instance the convection effect is equivalent to heat conduction. This could be determined from the balance between the advection term and diffusion term of the energy equation, which gives

$$u_z \frac{\Delta T}{L} \sim \kappa \frac{1}{R + 0.5\delta_t} \frac{1}{\delta_t} \left[\frac{(R + C_3\delta_t)\Delta T}{\delta_t} \right]. \quad (17)$$

By inserting the scale relations of u_z and δ_t , Eqs. (16) and (11), we could arrive at the following scale, where the subscript s denotes steady-state value:

$$t_s \sim \frac{L^2}{\kappa} \frac{1 + Pr^{-1/2}}{Ra^{1/2}} \frac{(R + C_3\delta_{ts})^{1/2}(R + 0.5\delta_{ts})^{1/2}}{R + 0.3\delta_{ts}}. \quad (18)$$

By adopting the aforementioned approach, the following variable Ψ_3 is proposed and employed to determine the coefficient C_3 :

$$\Psi_3(C_3) = \frac{\frac{L^2}{\kappa} \frac{1 + Pr^{-1/2}}{Ra^{1/2}} \frac{(R + C_3\delta_{ts})^{1/2}(R + 0.5\delta_{ts})^{1/2}}{R + 0.3\delta_{ts}}}{t_s}. \quad (19)$$

The numerically calculated standard deviation of Ψ_3 is presented in Fig. 7, where the Rayleigh number 10^8 , Prandtl number 10, and L/R from 100 to 1 are again employed.

It is clear in this figure that the value of C_3 could be determined as 0.37. This subsequently leads to

$$t_s \sim \frac{L^2}{\kappa} \frac{1 + Pr^{-1/2}}{Ra^{1/2}} \frac{(R + 0.37\delta_{ts})^{1/2}(R + 0.5\delta_{ts})^{1/2}}{R + 0.3\delta_{ts}}. \quad (20)$$

It is seen that Eq. (20) is also an implicit equation, and it reveals the relation between the thickness of the steady-state thermal boundary layer and the time to reach such a flow condition. It is also worth noting that t_s for thermal boundary layer flow developing at flat plates takes an explicit form $t_s \sim L^2\kappa^{-1}Ra^{-1/2}(1 + Pr^{-1/2})$; see, e.g., [19]. In comparison to the derived scale relation (20), it is inferred that the term $(R + 0.37\delta_{ts})^{1/2}(R + 0.5\delta_{ts})^{1/2}/(R + 0.3\delta_{ts})$ reflects the effect of the curvature of the heated surface.

B. Steady state

After the initial growth, the boundary layer will eventually transition to a steady state, in which the flow variables do not change temporally. The transient terms in the governing Eqs. (2) and (3) could be consequently ignored. Hence, for the steady-state boundary layer flow, by substituting the differential operators, Eq. (3) may be estimated as

$$u_{rs} \frac{\Delta T}{\delta_{ts}} + u_{zs} \frac{\Delta T}{L} \sim \kappa \frac{1}{(R + 0.5\delta_{ts})\delta_{ts}} \frac{R_4\Delta T}{\delta_{ts}}. \quad (21)$$

As argued above, the derivative term $(r\partial T/\partial r)$ cannot be simply quantified by $R\Delta T/\delta_{ts}$ for the present curved boundary layer flow. Hereby, the numerator r in $(r\partial T/\partial r)$ is estimated by R_4 , which is to be determined by the radius R and δ_{ts} . The scale of u_{zs} could be obtained by inserting Eq. (5) into Eq. (21), which gives

$$u_{zs} \sim \frac{\kappa L}{\delta_{ts}^2} \frac{R_4}{R + 0.5\delta_{ts}} \frac{1}{\frac{R + 0.5\delta_{ts}}{R + \delta_{ts}} + 1}. \quad (22)$$

We assume the coefficient R_4 in Eq. (22) is also in the form $R + C_4\delta_{ts}$. Likewise, the constant C_4 is decided from the seven case runs of our simulations at a Rayleigh number 10^8 , Prandtl number 10, and L/R ranging from 100 to 1. Figure 8 illustrates the associated regression process, and C_4 is herein determined to be 0.33. At this point, it is worth noting that $C_4 = 0.33$ does also hold for other flow conditions:

$$\Psi_4(C_4) = \frac{\frac{\kappa L}{\delta_{ts}^2} \frac{R+C_4\delta_{ts}}{R+0.5\delta_{ts}} \frac{1}{\frac{R+0.5\delta_{ts}}{R+\delta_{ts}} + 1}}{u_{zs}}. \quad (23)$$

Therefore, u_{zs} could be correlated with δ_{ts} by

$$u_{zs} \sim \frac{\kappa L}{\delta_{ts}^2} \frac{R + 0.33\delta_{ts}}{R + 0.5\delta_{ts}} \frac{1}{\frac{R+0.5\delta_{ts}}{R+\delta_{ts}} + 1}. \quad (24)$$

For the present fluid with a Prandtl number larger than the unity, the momentum of the convective flow is dominated by the viscous and buoyancy effects. By balancing the two terms in Eq. (2), the dominance of the boundary layer flow could be expressed by

$$\nu \frac{1}{(R + 0.5\delta_{vis})\delta_{vis}} \frac{R_5 u_{zs}}{\delta_{vis}} \sim g\beta \Delta T. \quad (25)$$

In Eq. (25), δ_{vis} is the location that corresponds to the maximum u_z at the steady state of the convective flow. By incorporating the relation $\delta_{vis} \sim \delta_{ts}/(1 + \text{Pr}^{-1/2})$ and assuming R_5 is in the form $R + C_5\delta_{vis}$, a parameter Ψ_5 could be therefore defined as

$$\Psi_5(C_5) = \frac{\left[\frac{\nu u_{zs} \frac{R+C_5\delta_{vis}}{(R+0.5\delta_{vis})} (1+\text{Pr}^{-1/2})^2}{g\beta \Delta T} \right]^{1/2}}{\delta_{ts}}. \quad (26)$$

Standard deviation of Ψ_5 is plotted at various C_5 in Fig. 9. This figure suggests that the minimum $\sigma(\Psi_5)$ is obtained at approximately $C_5 = 0.727$. Therefore, C_5 is determined to be 0.727. Note that the seven case runs employed for identifying $C_1 \sim C_4$ are also utilized for determining C_5 here. Hence, Eq. (25) is reduced to

$$\nu \frac{(R + 0.727\delta_{vis})}{(R + 0.5\delta_{vis})} \frac{u_{zs}}{\delta_{ts}^2} (1 + \text{Pr}^{-1/2})^2 \sim g\beta \Delta T. \quad (27)$$

It needs to mention that each of the above determined coefficients, C_1 – C_5 , is designed to obtain one scale law, and they are not utilized at the same time to describe one flow parameter. Hence, five coefficients in total are involved in this work to quantify different flow parameters and the curvature effect at various flow states.

By inserting Eq. (24) to Eq. (27), thickness of the steady-state boundary layer may be described by

$$\delta_{ts} \sim \frac{L(1 + \text{Pr}^{-1/2})^{1/2}}{\text{Ra}^{1/4}} \left\{ \frac{(R + 0.33\delta_{ts})[R(1 + \text{Pr}^{-1/2}) + 0.727\delta_{ts}]}{(R + 0.5\delta_{ts})[R(1 + \text{Pr}^{-1/2}) + 0.5\delta_{ts}]} \frac{1}{\frac{R+0.5\delta_{ts}}{R+\delta_{ts}} + 1} \right\}^{1/4}. \quad (28)$$

It is seen that Eq. (28) is implicit, and the least-square method could be utilized to obtain the scale of the steady-state boundary layer thickness, δ_{ts} . It is, however, crucial to note that a direct estimation of δ_{ts} by Eq. (28) will not be justified since correctly accounting for this equation requires an equal sign equation rather than an order of magnitude sign equation, which is similar to the above derivation of Eq. (12). In this aspect, to precisely obtain the scale of boundary layer thickness δ_{ts} , which will also be employed to obtain u_{zs} , we must know the exact form of Eq. (28). This is also achieved by processing our simulation data of the seven cases with a Rayleigh number 10^8 , Prandtl number 10, and L/R ranging from 100 to 1. Figure 10 depicts and compares the numerically obtained δ_{ts} values against the scale law in Eq. (28). A linear fit correlation is clearly shown in this

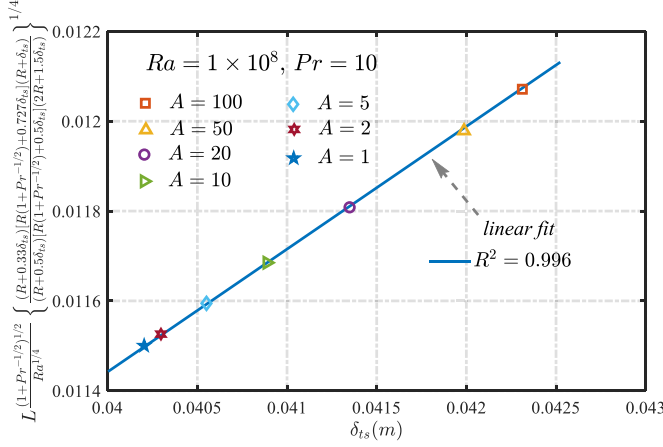


FIG. 10. Numerically calculated δ_{ts} vs its scale law in Eq. (28).

figure. Also, it is also revealed that a coefficient of 3.5 is appropriate, and the corresponding R^2 of the linear fit reaches 0.996. Therefore, the exact form of Eq. (28) could be achieved as

$$\delta_{ts} = 3.5 \frac{L(1 + \text{Pr}^{-1/2})^{1/2}}{\text{Ra}^{1/4}} \left\{ \frac{(R + 0.33\delta_{ts})[R(1 + \text{Pr}^{-1/2}) + 0.727\delta_{ts}]}{(R + 0.5\delta_{ts})[R(1 + \text{Pr}^{-1/2}) + 0.5\delta_{ts}]} \frac{1}{\frac{R+0.5\delta_{ts}}{R+\delta_{ts}} + 1} \right\}^{1/4}. \quad (29)$$

Hence, in order to determine the scaling-predicted steady-state δ_{ts} , one needs to iteratively resolve the implicit Eq. (29). Subsequently, the scaling-predicted characteristic velocity in the curved boundary layer flow, u_{zs} , is obtained by inserting δ_{ts} into Eq. (24).

It is seen in Eqs. (28) and (24) that when the radius of the cylinder approaches a very large value, the thickness and characteristic velocity of the convective boundary layer will converge to the following forms:

$$\delta_{ts} \sim \frac{L(1 + \text{Pr}^{-1/2})^{1/2}}{\text{Ra}^{1/4}}, \quad (30)$$

$$u_{zs} \sim \frac{\kappa L}{\delta_{ts}^2} \sim \frac{\kappa \text{Ra}^{1/2}}{L(1 + \text{Pr}^{-1/2})}. \quad (31)$$

Note that they are, in fact, the scales for thermal boundary layer at vertical flat plates proposed in [1,19], in which scenario the curvature of the surface does not affect the boundary layer flow at all. Hence, the $(R + N\delta_t)^m$ terms in Eqs. (28) and (24) could be considered as the manifestation of curvature effect of the circular cylinder.

C. Implementation of the proposed scale laws

In comparison to the well-known scaling relations of the convective boundary layers adjacent to flat plates, most of the above derived scale laws are implicit, and this results in a different sequence in applying and utilizing these scaling relations. Therefore, it is crucial to elaborate and clarify the scheme of scale-law implementation in this subsection.

For the initial growth of the convective boundary layer, the prioritized task is to determine the temporal growth of its thickness and characteristic velocity, that is, to determine δ_t and u_z at any specific evolutionary time instance t . To achieve this, Eq. (12) is first invoked and the exact solution of δ_t is obtained by, for example, a numerically iterative approach. Subsequently, the scale of the characteristic velocity u_z is determined by inserting δ_t into Eq. (16).

TABLE II. Sequence of implementation of the proposed unified scale laws.

Flow state	Variables and the corresponding scale laws	Scheme
a. Transient	$\delta_t \left(\frac{R+0.5\delta_t}{R+0.3\delta_t} \right)^{1/2} = 3.7\kappa^{1/2}t^{1/2}$	Exact
	$u_z \sim \frac{g\beta\Delta T t}{(1+\text{Pr}^{1/2})^2} \left(\frac{R+0.3\delta_t}{R+0.5\delta_t} \right)$	Scaling
b. Steady	$\delta_{ts} = 3.5 \frac{L(1+\text{Pr}^{-1/2})^{1/2}}{\text{Ra}^{1/4}} \left\{ \frac{(R+0.33\delta_{ts})(R(1+\text{Pr}^{-1/2})+0.727\delta_{ts})}{(R+0.5\delta_{ts})(R(1+\text{Pr}^{-1/2})+0.5\delta_{ts})} \frac{1}{\frac{R+0.5\delta_{ts}}{R+\delta_{ts}}+1} \right\}^{1/4}$	Exact
	$u_{zs} \sim \frac{\kappa L}{\delta_{ts}^2} \frac{R+0.33\delta_{ts}}{R+0.5\delta_{ts}} \frac{1}{\frac{R+0.5\delta_{ts}}{R+\delta_{ts}}+1}$	Scaling
c. Cutoff time for initial growth	$t_s \sim \frac{L^2}{\kappa} \frac{1+\text{Pr}^{-1/2}}{\text{Ra}^{1/2}} \frac{(R+0.37\delta_{ts})^{1/2}(R+0.5\delta_{ts})^{1/2}}{R+0.3\delta_{ts}}$	scaling

After the boundary layer reaches a steady state, its thickness and velocity do not vary with time any longer. Similar to the initial growth state, thickness of the steady-state boundary layer δ_{ts} is decided from the equation with an equal sign, i.e., Eq. (29). Then the scale of the steady-state boundary layer velocity u_{zs} is obtained by substituting δ_{ts} into Eq. (24).

As the scale of threshold time for the steady state t_s is implicitly correlated with δ_{ts} and u_{zs} , it could only be determined towards the very end. This could now be simply achieved by utilizing Eq. (20).

To better demonstrate how the present scale laws should be implemented and utilized, Table II details the corresponding sequence and scheme.

IV. VALIDATION OF THE PROPOSED SCALE LAWS

It is worth mentioning at this point that in this validation section, plain denotations stand for the numerically obtained values, while primed symbols denote the results determined from the present scale laws. That is, for instance, δ_t is obtained from numerical simulations, and δ'_t is decided from the proposed scale law. It also needs to clarify that determination of the primed scale variables in this section exactly follows the procedure and sequence elaborated in Table II. In the present validation section, variable dependency of the proposed scale law is validated separately, which is consistent with previous works; see, e.g., [22,39].

A. Initial growth

Figure 11(a) plots the numerically obtained boundary layer thickness δ_t against evolutionary time t . It is found that the boundary layer under all flow conditions experiences a transient and a steady state. Oscillations and overshoot in the thickness are observed in the LEE-dominated oscillatory state, and this is induced by the convective instability associated with the first group of unstable waves in the boundary layer, namely, the leading edge effect. Figure 11(b) depicts a rescaled version by normalizing the ordinate with the scale-law-predicted thickness at the steady state, δ'_{ts} , and the horizontal axis is normalized with the scale-law-predicted t_s . Figure 11(b) clearly demonstrates that all data almost collapse together with the three development states clearly shown. This also suggests the proposed temporal development of boundary layer thickness indicated in Eq. (12), the relation describing the steady-state boundary layer thickness, Eq. (29), and the time to reach steady state, Eq. (20), are correct. Figure 11(b) also demonstrates that the present boundary layer thickness grows with $t^{1/2}$. It is worth noting that, unlike the flat-plate boundary layers, this dependency is not immediately discernible from the corresponding scale law in Eq. (12).

Temporal evolution of the characteristic velocity in the thermal boundary layer is presented in Fig. 12, where Fig. 12(a) plots the original raw data and the normalized results are given in Fig. 12(b). Similar to the development of boundary layer thickness, this figure suggests that the characteristic velocity also undergoes a transient and a steady state. The numerically obtained characteristic velocities are normalized by the scale-law-predicted steady-state u_{zs} , and the dimensional

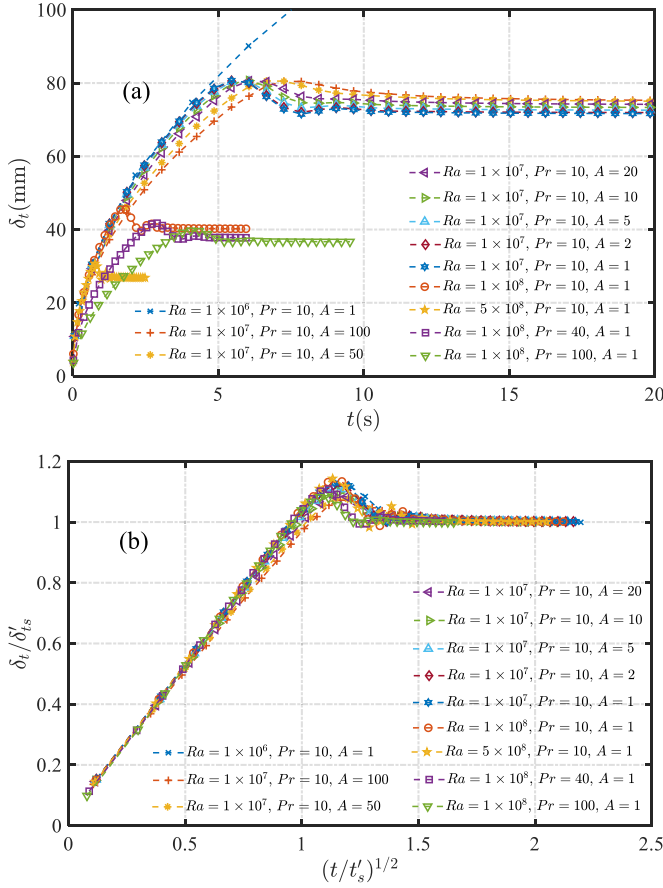


FIG. 11. Time series of thickness of the curved thermal boundary layer: (a) raw data, (b) normalized results.

evolutionary time is divided by the scale-law-predicted t_s in Fig. 12(b). It is seen that, by doing such, all data converge together. It is also found that the characteristic velocity increases linearly with time in the initial growth state, which is the same as the flat-plate boundary layers. It is worth mentioning that, unlike the flat-plate boundary layers, this linear growth does not immediately manifest itself from the scale law in Eq. (16), since u_z is implicitly correlated with both thickness and time. Nevertheless, the collapse of all calculated data strongly suggests that the proposed scale relation for the boundary layer thickness in Eq. (16), the scale law describing the steady-state boundary layer thickness in Eq. (24), and the time to reach steady state in Eq. (20) are revealing the correct flow mechanics.

As argued in Sec. III, correctly and precisely accounting for flow quantities crucially depends on determination of the balance between the various terms of the governing equations. Figure 13(a) compares the horizontal profiles of the unsteady, diffusion, streamwise advection, and radial advection terms of the energy equation. Note that the case that corresponds to the highest curvature effect is utilized here, since the opposite situation, the flat-plate condition, has been intensively studied in the literature. It is clearly seen in Fig. 13(a) that the unsteady term and diffusion terms are much more important than the other terms, which validates and supports the balance for analyzing the boundary layer thickness in the initial growth state. Likewise, various terms of the momentum equation, i.e., the diffusion term, buoyancy term, unsteady term, streamwise advection, and radial advection terms, are plotted in Fig. 13(b) for the initial growth state. It is found that the buoyancy

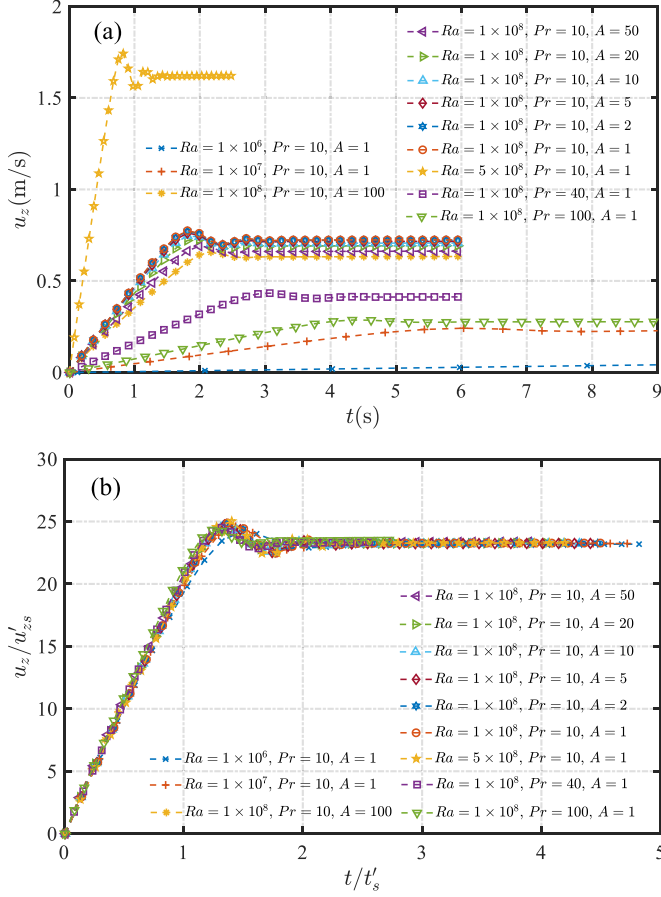


FIG. 12. Time series of characteristic velocity of the curved thermal boundary layer: (a) raw data, (b) normalized results.

and diffusion terms are the most important, and the flow is subsequently dominated by these two effects. This is consistent with and validates the force balance utilized for deriving Eq. (16).

B. Steady state

Thickness and characteristic velocity do not vary with time when the convective boundary layer eventually reaches the steady state. Our scale analysis suggests that the boundary layer thickness could be quantified by Eq. (29). Figure 14 compares the numerically calculated values against the scale-law-predicted data at various Ra , Pr , and A . A linear fit line is clearly seen, and it implies that the proposed Eq. (29) could suitably address the thickness of the curved boundary layer flow in the steady state.

Figure 15 plots the numerically obtained characteristic velocities against the scale-law-predicted values at various Ra , Pr , and A . It is seen that the two sets of data compare favorably well, and all data fall onto the same linear fitted line. This suggests that the proposed scale relation in Eq. (24) could appropriately describe the momentum of the curved boundary layer flow.

In the analysis of the steady-state energy equation in Sec. III, we utilized the balance between the summation of the two advection terms and the diffusion term, which physically means the heat conducted through the curved surface is convected away both radially and axially by the curved

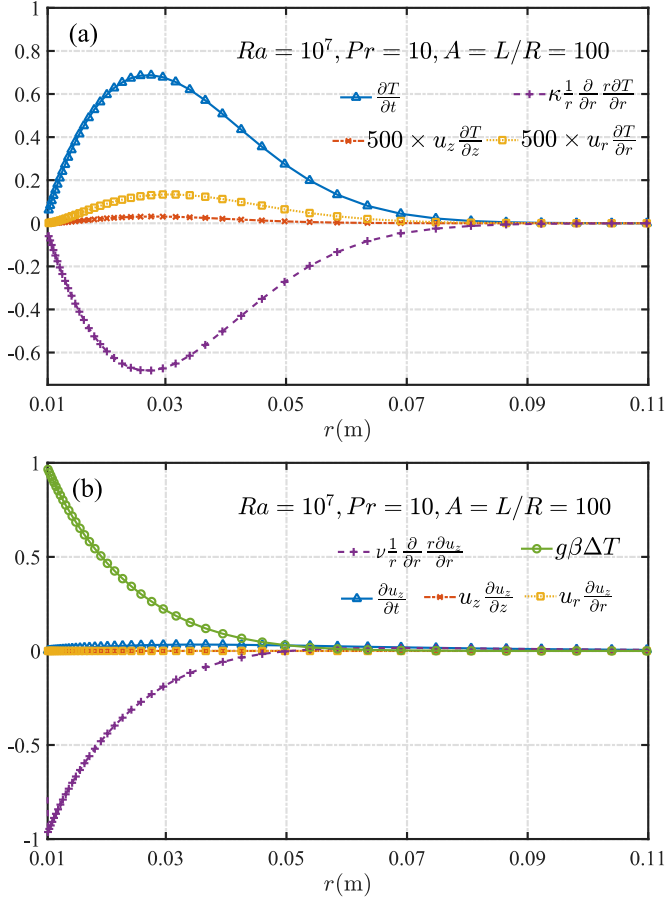


FIG. 13. Horizontal profiles of the various terms of the governing equations, obtained with $Ra = 1 \times 10^7$, $Pr = 10$, $A = 100$ and at a streamwise location $z = L$ ($t = 0.3286t_s$): (a) energy equation, (b) streamwise momentum equation.

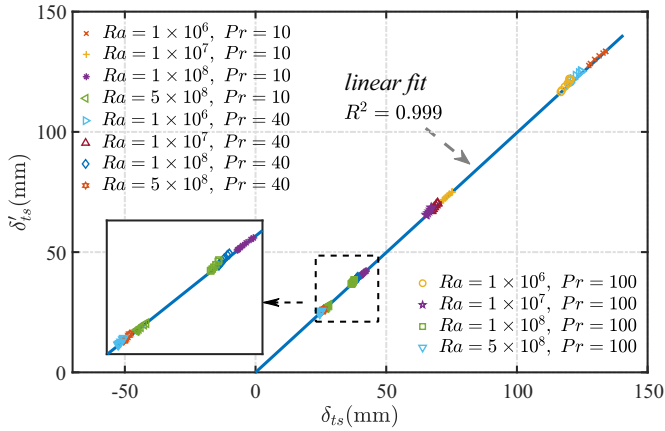


FIG. 14. Numerically obtained δ_{ls} vs the scaling-law predicted δ'_{ls} ($A = 100, 50, 20, 10, 5, 2, 1$).

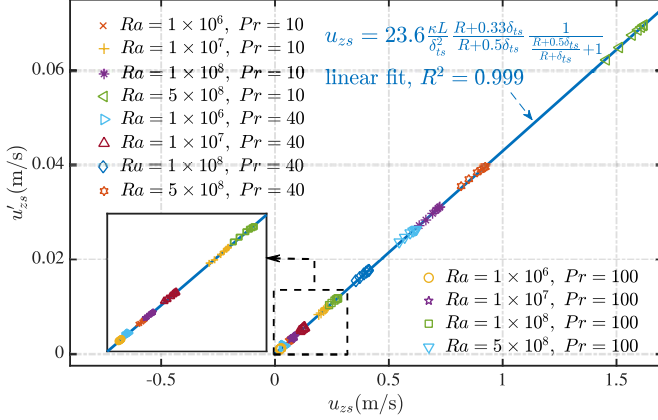


FIG. 15. Numerically obtained u_{zs} vs the scale-law-predicted u'_{zs} ($A = 100, 50, 20, 10, 5, 2, 1$).

boundary layer. Figure 16(a) depicts horizontal profiles of the various terms of the energy equation in the steady state with the case $Ra = 1 \times 10^7$, $Pr = 10$, and $R = L/100$. This figure demonstrates that the diffusion term, which corresponds to heat conduction, is the most important factor of the flow, while the two advection terms are of equivalent but slightly less significance in comparison. Nevertheless, summation of the two advection terms is at the same order of the diffusion term. Consequently, it validates the balance adopted for analyzing the energy equation at the steady state. It is also seen that the unsteady term is zero, indicating the steady-state flow does not depend on time. Likewise, Fig. 16(b) presents the comparison of various terms of the momentum equation. It clearly shows that the buoyancy effect and the momentum diffusion are of similar importance and all other effects could be hereby ignored, which supports and is consistent with the dominance we utilized in Eq. (25).

The scale-law-determined t'_s is plotted against the numerically calculated values at various Ra , Pr , and A in Fig. 17. A linear fit line is clear, and the regression constant is 0.999, suggesting the proposed scale relation in Eq. (20) is sound and reasonable. It is worth mentioning that in the numerical simulation, t_s is determined at the time instance when the characteristic velocity in the boundary layer reaches 95% of its steady-state value at the streamwise location $z = L$, and a similar approach was utilized in [16,21,39].

C. Effect of curvature on boundary layer flow

It has been widely acknowledged in the literature that if the radius of the heated circular cylinder is much larger than the thickness of the thermal boundary layer, the curvature effect of the heated surface does not remarkably affect the flow and is negligible accordingly. In this scenario, we will have a flat boundary layer. However, if the radius of the cylinder is equivalent or smaller than the boundary layer thickness, the curvature effect will then profoundly affect the boundary layer, and it will subsequently lead to a curved boundary layer. Here a dimensionless parameter ξ is defined to straightforwardly address the effect of curvature:

$$\xi = \frac{\delta_t}{R}. \quad (32)$$

As discussed above, the present study aims to account for the effect of curvature on the convective boundary layer, that is to provide a set of unified scale laws that is capable of describing the convective boundary layer flow covering large value range of cylinder radius. The scale analysis in Sec. III suggests that at the steady state, the boundary layer thickness could be described by Eq. (29), whereas the complex term $(R + 0.33\delta_{ts})(R + \delta_{ts})[R(1 + Pr^{-0.5}) + 0.727\delta_{ts}]$

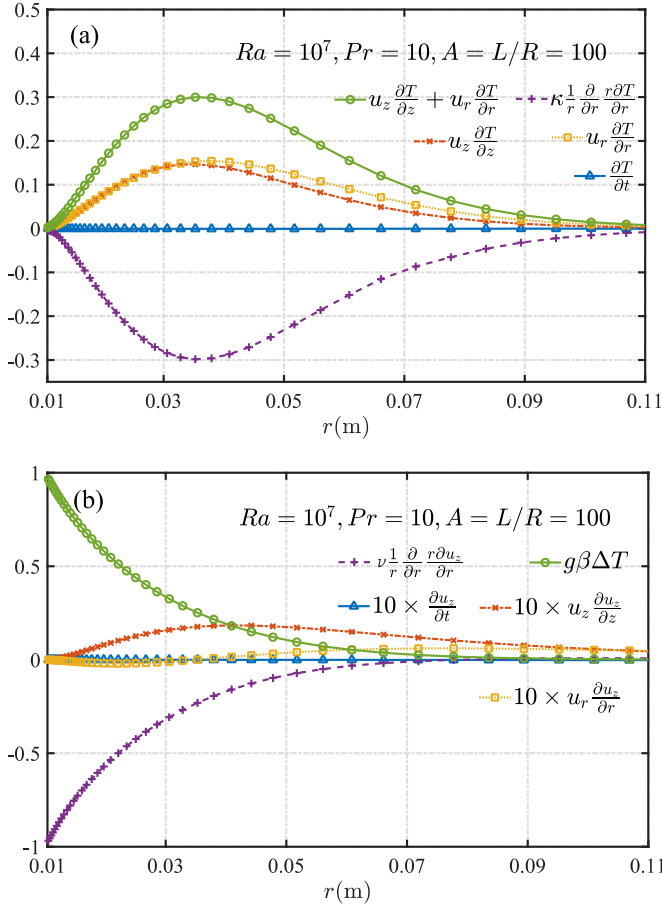


FIG. 16. Horizontal profiles of the various terms of the governing equations, obtained with $Ra = 1 \times 10^7$, $Pr = 10$, $A = 100$ and at a streamwise location $z = L$ ($t = 6.37t_s$): (a) energy equation, (b) streamwise momentum equation.

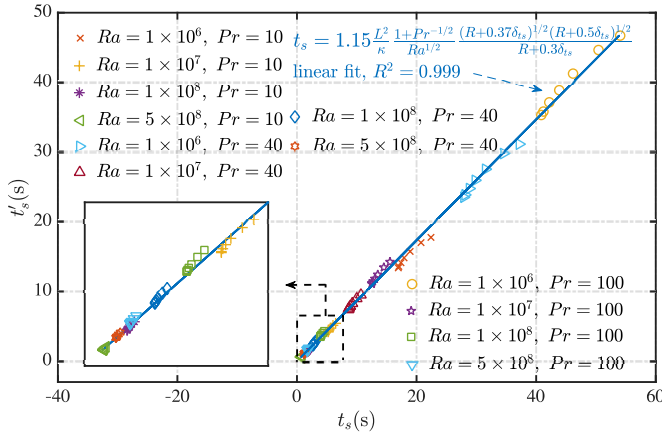


FIG. 17. Numerically obtained t_s against its scale-law-determined t'_s .

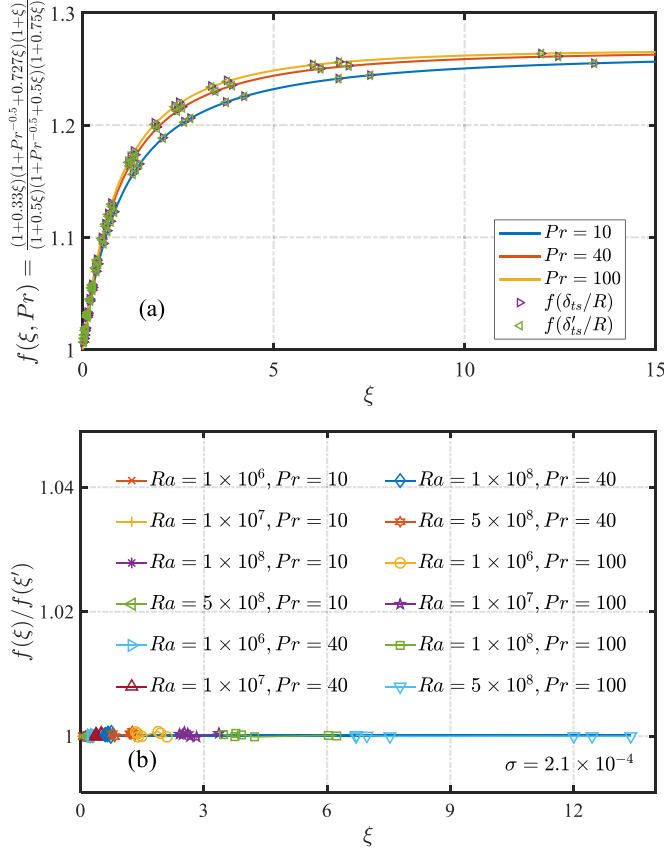


FIG. 18. Effect of curvature on the thickness of boundary layer flow at various ξ : (a) $f(\xi)$ vs ξ , (b) $f(\xi)/f(\xi')$ vs ξ .

$(R + 0.5\delta_{ts})(R + 0.75\delta_{ts})[R(1 + Pr^{-0.5}) + 0.5\delta_{ts}]$ denotes the curvature effect at different radius. To better understand the curvature effect of the heated surface, the following function could be defined:

$$f(\xi, Pr) = \frac{(1 + 0.33\xi)(1 + \xi)(1 + Pr^{-1/2} + 0.727\xi)}{(1 + 0.5\xi)(1 + 0.75\xi)(1 + Pr^{-1/2} + 0.5\xi)}. \quad (33)$$

In the above equation, we could obtain a ξ value for each calculated case run. The effect of curvature is associated with ξ and reflected by the term $f(\xi, Pr)$. Note that the scale for the thickness of flat boundary layers is $\delta_{ts} \sim L(1 + Pr^{-1/2})^{1/2}/Ra^{1/4}$. For the present curved boundary layers, it takes the form of Eq. (28), in which the $\delta_{ts} \sim L(1 + Pr^{-1/2})^{1/2}/Ra^{1/4}$ term corresponds to the flat boundary layer scale, and the complicated $(R + N\delta_t)$ term indicates the effect of the present curvature effect. To examine the curvature effect in a straightforward way and to demonstrate that the present unified laws work well at all curvature effects, i.e., at small ξ , intermediate ξ , and large ξ , we herein define the complicated $(R + N\delta_t)$ term as $f(\xi, Pr)$ since it is also Prandtl number dependent. It is plotted against ξ at various Pr numbers for this purpose. On the one hand, when ξ approaches infinitesimal, the flow becomes a flat-plate problem, we have $\lim_{\xi \rightarrow 0} f(\xi, Pr) = 1$, and the scale laws in Table II will reduce to the flat-plate scalings. On the other hand, when ξ is very large, i.e., the boundary layer is much thicker than the radius of the cylinder, $f(\xi, Pr)$ will also approach a constant. Figure 18(a) plots $f(\xi, Pr)$ at three Pr numbers. Note that both the numerically obtained and scale-law-predicted values are presented in this figure, and the solid line is a direct plot of the

function in Eq. (33). It is clear that the three data clusters almost converge together, indicating the proposed scale laws are consistent with the numerical simulations. This figure demonstrates that the proposed scale law is unified, and it could appropriately describe the limiting cases of flat boundary layer (at small ξ) and significantly curved boundary layer (at large ξ) as well as all intermediate ξ . It is also worth pointing out in this figure that $f(\xi, \text{Pr})$, which represents the deviation of curved boundary layer from the flat-plate flow, increases drastically with ξ at $0 < \xi < 5$ in the first place. Then it steadily approaches a constant of approximately 1.23. This figure also suggests that the maximum ξ in the present study reaches approximately 14, suggesting the maximum boundary layer thickness is 14 times the cylinder radius, in which case the convective boundary layer has become a dramatically curved one [see Fig. 1(a)]. At the other end, the minimum ξ is approximately 0.02 indicating a flat-plate problem, in which scenario a good agreement is also achieved. It is worth noting the minimum ξ is found to be 0.02 for the case run with $\text{Ra} = 5 \times 10^8$, $\text{Pr} = 100$, and $A = 1$. Consequently, it is known that the present scale laws could reasonably quantify the boundary layer thickness for a large range of ξ .

In order to precisely and quantitatively examine the difference between the numerical simulations and the proposed scale laws, Fig. 18(b) presents the ratio of $f(\xi, \text{Pr})$ and $f(\xi', \text{Pr})$ at various ξ . The comparison demonstrates that the present scale-law-predicted values agree well with the numerical results and the relative error is below 1%, validating the proposed scale law in Eq. (29).

Similar to the above discussion of the curvature effect on boundary layer thickness, the following function $g(\xi)$ is defined to expound the effect of curvature on the characteristic velocity. It is noted that this function is chosen from Eq. (24):

$$g(\xi) = \frac{(1 + 0.33\xi)}{(1 + 0.5\xi)} \frac{1}{\frac{(1+0.5\xi)}{(1+\xi)} + 1}. \quad (34)$$

Similar to the above $f(\xi)$, in Eq. (34), we could obtain a ξ value for each calculated case run. The effect of curvature on the characteristic velocity is associated with ξ and reflected by the term $g(\xi)$. Values of $g(\xi)$ are obtained at various ξ from the present numerical simulations and from the proposed scale laws. The corresponding data are plotted in Fig. 19(a), where the solid line is by directly calculating the function $g(\xi)$. This figure shows that the proposed scale law could reasonably describe the limiting cases of flat boundary layer (at small ξ) and highly curved boundary layer (at large ξ) as well as intermediate ξ . When ξ approaches zero, that is, when the boundary layer thickness is much smaller than the radius of the cylinder, the flow is reduced to flat-plate problems. In this situation, we have $\lim_{\xi \rightarrow 0} g(\xi) = 0.5$, and this is consistent with Fig. 19(a). However, when the boundary layer thickness is significantly larger than the radius of the cylinder, $\xi \gg 1$, $g(\xi)$ also gradually approaches a constant. Figure 19(b) plots the ratio $g(\xi)/g(\xi')$ against ξ . It is seen that the agreement is reasonable with the maximum relative error at approximately 0.3%. It is also clear in Figs. 19(a) and 19(b) that the three sets of data almost collapse together covering a wide range of thickness-radius ratio, at $0.02 \leq \xi \leq 14$. This suggests the proposed scale law in Eq. (24) could properly account for the curvature effect.

To assess how precisely the present scale law describes the curvature effect in a more direct and straightforward way, Fig. 20 plots the ratio of the numerically obtained flow parameters against the scale-law-predicted values at various ξ , where Figs. 20(a) and 20(b) depict the boundary layer thickness and characteristic velocity data, respectively. It demonstrates that the present scale-law-predicted values are in good agreement with the numerical simulations, and this consequently suggests that the present unified scale laws could accurately account for the boundary layer flow from the extensively investigated flat-plate type to a strongly curved one, covering $0.02 \leq \xi \leq 14$.

The above discussion suggests that the present scale laws could reasonably address $0.02 \leq \xi \leq 14$. It is worth pointing out that this data range as well as the associated scale laws are in fact determined by the corresponding case runs analyzed, i.e., by numerically obtaining the coefficients $C_1 \sim C_5$. Therefore, it makes perfect sense that the proposed scale laws could satisfactorily describe these flow conditions. It is obvious that the present scale laws are still valid when ξ is further lower

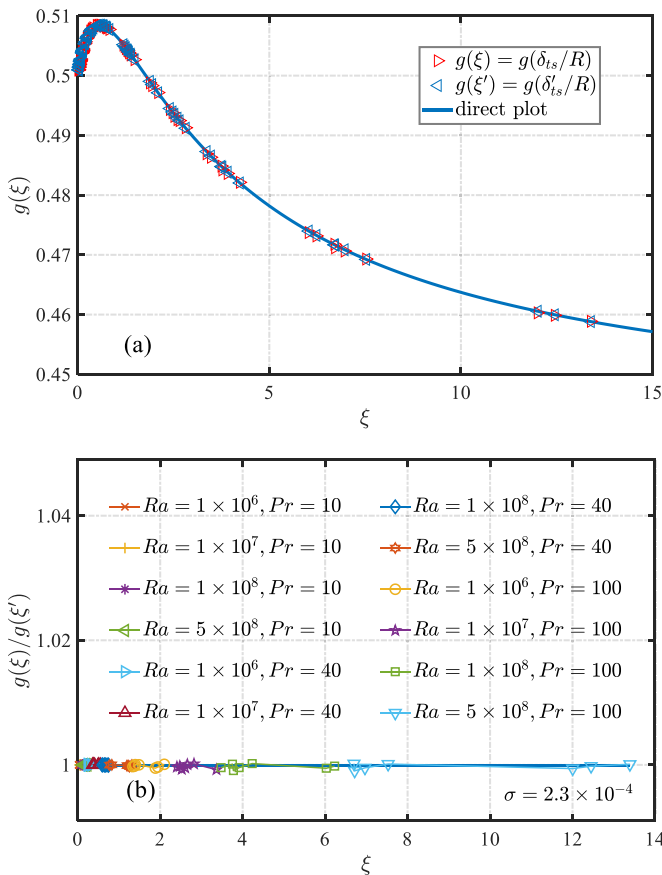


FIG. 19. Effect of curvature on the characteristic velocity of boundary layer flow at various ξ . (a) $g(\xi)$ vs ξ . (b) $g(\xi)/g(\xi')$.

and closer to the unity. How the present scale laws perform at higher ξ could be an interesting question, as one may expect the present scale laws should still be valid at least to some extent beyond the upper limit $\xi = 14$. An increase in ξ corresponds to an augmented curvature effect, and this could be achieved by further decreasing the cylinder radius or reducing the Rayleigh number. In this aspect, we have further calculated and examined several additional cases, and the maximum ξ tested is equal to 26. The scale-law-predicted thickness and characteristic velocity differentiate from simulation values by up to 0.26% and 6.28%, respectively, for $14 \leq \xi \leq 26$. This implies that the present scale laws could practically describe the boundary layers at $0 \leq \xi \leq 26$ with satisfactory agreement. In the upper limiting case, $\xi = 26$, the boundary layer thickness is about 26 times the cylinder radius, and the cylinder has almost been reduced to a line heat source. In the lower limiting case, however, the boundary layer becomes the traditional flat boundary layer.

V. CONCLUDING REMARKS

This work investigates the convective boundary layer flow developing along the external surface of a vertical circular cylinder by means of scale-law analysis. The effect of curvature is taken into account by adopting different aspect ratios of the employed heated cylinder. Large variation of the cylinder aspect ratio, $1 \leq A \leq 100$, is considered, and it leads from a most curved boundary layer

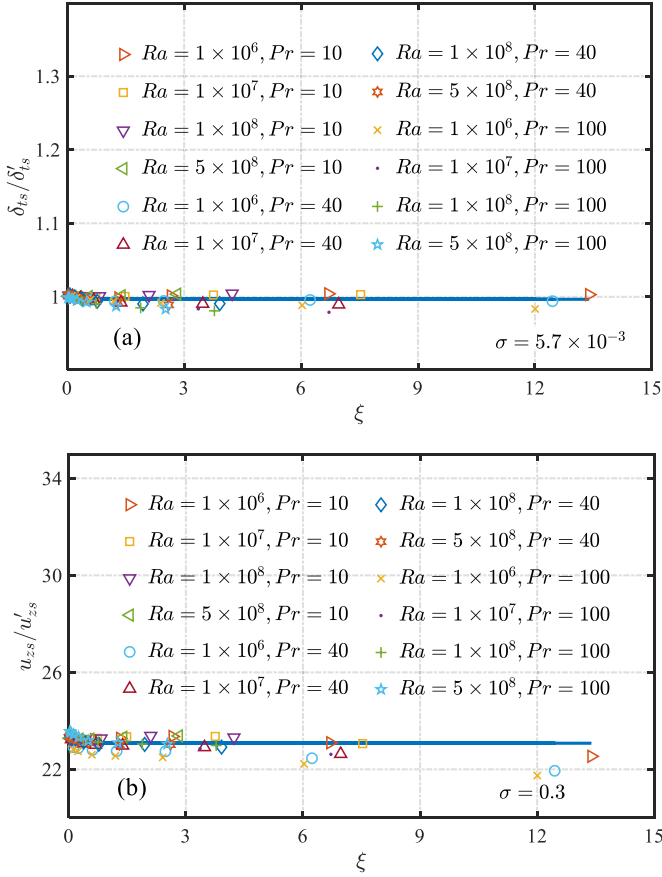


FIG. 20. Comparison of the numerically determined flow variables against the scale-law-predicted ones at various ξ : (a) $\delta_{ts} / \delta'_{ts}$, (b) u_{zs} / u'_{zs} .

at approximately $\xi \approx 14$ [refer to Fig. 1(a)] to an almost flat boundary layer at approximately $\xi \approx 0.02$. In the meantime, the Rayleigh number and Prandtl number dependencies are also resolved.

Two distinct flow states are revealed from the present simulations, a transient and a steady state. Through analyzing the various terms in the governing equations, we obtain the scale laws describing the thickness δ_t and characteristic velocity u_z in the initial growth state, the time to reach the steady state t_s , and the steady-state thickness δ_{ts} and characteristic velocity u_{zs} of the thermal boundary layer. It demonstrates that several scale laws are in an implicit form, and hence precisely evaluating the flow variables will need to utilize an iterative approach. The present study also suggests that if the radius of the cylinder is much larger or much smaller than the boundary layer thickness, the proposed scale laws will converge to the classic scaling relations for flat-plate problems. Nevertheless, when they are comparable, the traditional flat-plate scale laws will fail. It is also found that the proposed scale laws quantifying the curved boundary layer at various ξ generally resemble the classic flat-plate scaling relations. The various $(R + N\delta_t)^m$ terms in the scale laws act to calibrate the corresponding flat-plate relations towards curved ones, and they quantitatively describe the curvature effect.

The present study indicates that the proposed scale laws are capable of reasonably describing from flat boundary layers at $\xi = 0$ to remarkably curved ones at $\xi = 26$. The effect of the Rayleigh and Prandtl numbers could also be suitably quantified and described by the proposed scale laws.

Therefore, the present proposed relations are considered as generalized and unified scale laws for convective boundary layers developing along an isothermally heated vertical cylinder.

- [1] J. C. Patterson and J. Imberger, Unsteady natural convection in a rectangular cavity, *J. Fluid Mech.* **100**, 65 (1980).
- [2] L. Prandtl, On fluid flow with very little friction, in *Proceedings of 3rd International Congress of Mathematicians, Heidelberg, Germany* (B. G. Teubner, Leipzig, 1904), pp. 484–491.
- [3] H. Blasius, Grenzschichten in Flüssigkeiten mit kleiner Reibung (The boundary layers in fluids with little friction), *Zs. Angew. Math. Phys.* **56**, 1 (1908).
- [4] G. K. Batchelor, Heat transfer by free convection across a closed cavity between vertical boundaries at different temperatures, *Q. Appl. Math.* **12**, 209 (1954).
- [5] B. Gebhart and R. P. Dring, The leading edge effect in transient natural convection from a vertical plate, *J. Heat Transfer* **89**, 274 (1967).
- [6] T. Wei, Scaling of the production of turbulent kinetic energy and temperature variance in a differentially heated vertical channel, *Phys. Rev. Fluids* **4**, 081501(R) (2019).
- [7] Y. Liu and S. Ren, Receptivity of incompressible convective boundary layers induced by linear thermal forcing, *Phys. Fluids* **33**, 034127 (2021).
- [8] T. Anthony, Cylindrically symmetric diamond parts by hot-filament CVD, *Diamond Relat. Mater.* **6**, 1707 (1997).
- [9] J. Zhao, J. Liu, H. Dong, W. Zhao, and L. Wei, Numerical investigation on the flow and heat transfer characteristics of waxy crude oil during the tubular heating, *Intl J. Heat Mass Transfer* **161**, 120239 (2020).
- [10] Z. Wu, L. Hou, S. Wu, X. Wu, and F. Liu, The time-to-failure assessment of large crude oil storage tank exposed to pool fire, *Fire Safety J.* **117**, 103192 (2020).
- [11] I. Langmuir, Convection and conduction of heat in gases, *Phys. Rev. Series I* **34**, 401 (1912).
- [12] W. Elenbaas, The dissipation of heat by free convection from vertical and horizontal cylinders, *J. Appl. Phys.* **19**, 1148 (1948).
- [13] R. P. Dring and B. Gebhart, Transient natural convection from thin vertical cylinders, *J. Heat Transfer* **88**, 246 (1966).
- [14] W. J. Minkowycz and E. M. Sparrow, Local nonsimilar solutions for natural convection on a vertical cylinder, *J. Heat Transfer* **96**, 178 (1974).
- [15] H. Khouaja, T. S. Chen, and B. F. Armaly, Mixed convection along slender vertical cylinders with variable surface heat flux, *Intl J. Heat Mass Transfer* **34**, 315 (1991).
- [16] Y. Zhao, C. Lei, and J. C. Patterson, Magnified heat transfer from curved surfaces: A scaling prediction, *Phys. Fluids* **33**, 021702 (2021).
- [17] G. Kang, B. Chung, and H. Kim, Natural convection heat transfer on a vertical cylinder submerged in fluids having high Prandtl number, *Intl J. Heat Mass Transfer* **79**, 4 (2014).
- [18] A. Bejan, *Convection Heat Transfer* (Wiley, New York, 1984).
- [19] W. Lin, S. W. Armfield, J. C. Patterson, and C. Lei, Prandtl number scaling of unsteady natural convection boundary layers for $Pr > 1$ fluids under isothermal heating, *Phys. Rev. E* **79**, 066313 (2009).
- [20] Y. Liu, Y. Bian, Y. Zhao, S. Zhang, and Q. Suo, Scaling laws for the transient convective flow in a differentially and linearly heated rectangular cavity at $Pr > 1$, *Phys. Fluids* **31**, 043601 (2019).
- [21] Y. Liu, Scaling of convective boundary layer flow induced by linear thermal forcing at $Pr < 1$ and $Pr > 1$, *Phys. Rev. E* **100**, 043112 (2019).
- [22] Y. Liu and S. Ren, Improved scaling analysis of the transient buoyancy-driven flow induced by a linear temperature gradient, *Intl J. Heat Mass Transfer* **162**, 120386 (2020).
- [23] W. Lin and S. W. Armfield, Unsteady natural convection on an evenly heated vertical plate for Prandtl number $Pr < 1$, *Phys. Rev. E* **72**, 066309 (2005).

- [24] S. W. Armfield, J. C. Patterson, and W. Lin, Scaling investigation of the natural convection boundary layer on an evenly heated plate, *Intl J. Heat Mass Transfer* **50**, 1592 (2007).
- [25] W. Lin and S. W. Armfield, Scalings for unsteady natural convection boundary layers on an evenly heated plate with time-dependent heating flux, *Phys. Rev. E* **88**, 063013 (2013).
- [26] B. Nie and F. Xu, Scales of natural convection on a convectively heated vertical wall, *Phys. Fluids* **31**, 024107 (2019).
- [27] J. Ma, B. Nie, and F. Xu, Transient flows on an evenly heated wall with a fin, *Intl J. Heat Mass Transfer* **118**, 235 (2018).
- [28] G. Boffetta, M. Borgnino, and S. Musacchio, Scaling of Rayleigh-Taylor mixing in porous media, *Phys. Rev. Fluids* **5**, 062501 (2020).
- [29] A. Celani, A. Mazzino, and L. Vozella, Rayleigh-Taylor Turbulence in Two Dimensions, *Phys. Rev. Lett.* **96**, 134504 (2006).
- [30] G. Boffetta, A. Mazzino, S. Musacchio, and L. Vozella, Kolmogorov scaling and intermittency in Rayleigh-Taylor turbulence, *Phys. Rev. E* **79**, 065301 (2009).
- [31] G. Boffetta, M. Magnani, and S. Musacchio, Suppression of Rayleigh-Taylor turbulence by time-periodic acceleration, *Phys. Rev. E* **99**, 033110 (2019).
- [32] S. Grossmann and D. Lohse, Thermal Convection for Large Prandtl Numbers, *Phys. Rev. Lett.* **86**, 3316 (2001).
- [33] O. Shishkina, M. S. Emran, S. Grossmann, and D. Lohse, Scaling relations in large-Prandtl-number natural thermal convection, *Phys. Rev. Fluids* **2**, 103502 (2017).
- [34] B. Miquel, S. Lepot, V. Bouillaut, and B. Gallet, Convection driven by internal heat sources and sinks: Heat transport beyond the mixing-length or “ultimate” scaling regime, *Phys. Rev. Fluids* **4**, 121501 (2019).
- [35] T. Wei, Scaling of Reynolds stresses in a differentially heated vertical channel, *Phys. Rev. Fluids* **4**, 051501(R) (2019).
- [36] T. Wei, Scaling of turbulent kinetic energy and dissipation in turbulent wall-bounded flows, *Phys. Rev. Fluids* **5**, 094602 (2020).
- [37] Y. Liu and S. Ren, Scale law analysis of the curved boundary layer evolving around a horizontal cylinder at $Pr > 1$, *Phys. Fluids* **33**, 073614 (2021).
- [38] Y. Liu, C. Lei, and J. C. Patterson, Plume separation from an adiabatic horizontal thin fin placed at different heights on the sidewall of a differentially heated cavity, *Int. Commun. Heat Mass Transfer* **61**, 162 (2015).
- [39] W. Lin, S. W. Armfield, and P. Morgan, Unsteady natural convection boundary-layer flow along a vertical isothermal plate in a linearly stratified fluid with $Pr > 1$, *Intl J. Heat Mass Transfer* **45**, 451 (2002).